High Power RF Discharge Detection Technique Based on the In-Phase and Quadrature Signals

Oscar Monerris-Belda, Raúl Cervera Marín, Miguel Rodríguez Jodar, Elena Diaz-Caballero, Carlos Alcaide Guillén, John Petit, Vicente E. Boria, *Fellow, IEEE*, Benito Gimeno, *Member, IEEE*, and David Raboso

***Abstract*— High power radio frequency (RF) breakdown testing is a subject of great relevance in the space industry, due to the increasing need of higher transmission power and smaller devices. This work presents a novel RF breakdown detection system, which monitors the same parameters as the microwave nulling system but with several advantages. Where microwave nulling—a de facto standard in RF breakdown testing—is narrowband and requires continuous tuning to keep its sensitivity, the proposed technique is broadband and maintains its performance for any RF signal. On top of that, defining the detection threshold is cumbersome due to the lack of an international standardized criterion. Small responses may appear in the detection system during the test and, sometimes, it is not possible to determine if these are an actual RF breakdown or random noise. This new detection system uses a larger analysis bandwidth, thus reducing the cases in which a small response is difficult to be classified. The proposed detection method represents a major step forward in high power testing as it runs without human intervention, warning the operator or decreasing the RF power automatically much faster than any human operator.**

***Index Terms*— Corona, microwave devices, multipactor, radio frequency (RF) breakdown, RF high power.**

I. Introduction

MICROWAVE devices for space applications might suffer from radio frequency (RF) breakdown discharges, which only happen in reduced pressure or high vacuum conditions, the multipactor breakdown being of specific interest in this article [1]. Ensuring that the microwave and RF devices will not suffer from these effects is crucial as, once in orbit, the only option to mitigate them is to reduce the transmitted power, thus leading to a data throughput reduction, if not a total mission failure.

Multipactor discharge is a vacuum breakdown in which an initial electron present inside the structure can stimulate an avalanche of electrons. The region in which the discharge happens at the lowest RF power is known as the critical gap. The electron kinetic energy increases due to its interaction with the RF field and, due to the vacuum environment, it impacts on the device's inner surfaces. For a certain kinetic energy range, these collisions can release more than one electron, due to the material secondary emission [1], [2]. The RF breakdown happens when the number of electrons grows exponentially.

To produce robust RF component designs, multipactor simulation and testing must be done. Because of its high cost, testing must not be considered as an intermediate stage in the design process, but a final verification which certifies the correct operation of the device. However, with increasing complexity in terms of geometry [3], [4], materials [5], [6], and surface finishing, achieving accurate multipactor simulations becomes a challenge. Modeling tools have seen large advances recently [7]–[9], and simulations with modulated signal [10], [11], space charge [12], multiple materials [13], [14], or simple noise characterization [15] are common nowadays. All of these advances in the simulation field are driving designers to request that their devices are tested against the same conditions that they were simulated—in terms of RF power, signal modulation, and temperature [16].

When dealing with modulated signals, designers find that test routes and required detection systems are not properly specified in the international standards [17], [18]. Test sites have relied, for many years, on a set of local and global detection methods [19]–[21]. The drawback of these methods is that many of them have been developed for operation with continuous wave (CW) or pulsed CW signals.

The detection methods can be classified either in relation to their detection range—local and global methods [20], [21]—or to the type of measured physical parameter— RF signal magnitude at fundamental or harmonic frequencies, quantity of free electrons (electron current), emitted ultraviolet light, and pressure in the test environment.

The local detection methods are those which can detect the RF breakdown in the vicinity of the critical area and indicate

Manuscript received June 9, 2021; revised September 1, 2021; accepted September 11, 2021. Date of publication November 1, 2021; date of current version December 3, 2021. This work was supported in part by the "Ministerio de Ciencia e Innovación," Spanish Government, under Project PID2019-103982RB-C41, and in part by the European High RF Power Space Laboratory of the European Space Agency and Val Space Consortium for contributing with its installations, Laboratory co-funded by the European Regional Development Fund—A way of making Europe. *(Corresponding author: Oscar Monerris-Belda.)*

Oscar Monerris-Belda, Raúl Cervera Marín, Miguel Rodríguez Jodar, and John Petit are with Val Space Consortium, 46022 Valencia, Spain (e-mail: oscar.monerris@val-space.com).

Elena Diaz-Caballero, Carlos Alcaide Guillén, and Vicente E. Boria are with the Instituto de Telecomunicaciones y Aplicaciones Multimedia, Universitat Politècnica de València, 46022 Valencia, Spain.

Benito Gimeno is with the Instituto de Física Corpuscular (IFIC), and the Department of Applied Physics and Electromagnetics, CSIC-University of Valencia, 46100 Valencia, Spain.

David Raboso is with the European Space Research and Technology Centre, European Space Agency, 2200 Noordwijk, The Netherlands.

Color versions of one or more figures in this article are available at https://doi.org/10.1109/TMTT.2021.3120657.

Digital Object Identifier 10.1109/TMTT.2021.3120657

TABLE I
TYPICAL BACKGROUND NOISE AND MINIMUM CHANGE OF OUTPUT PARAMETERS FOR RELIABLE MULTIPACTOR DETECTION

Detection system	Background noise	Minimum change
Nulling	20 to 40 dBc	$5-10$ dB
Harmonic	>90 dBc	$5-10$ dB
Electron monitoring	$<10^{-11}$ A	$5-10$ dB
Light monitoring	<0.1 V	$5-10$ dB
Close to carrier noise	>40 dBc	>10 dB
Pressure	$<10^{-5}$ mbar	>10 dB

the critical gap location. Electron current and/or emitted light monitoring [17] are examples of local detection methods. However, global detection systems cannot determine where in the test system it has happened. Some of these methods are microwave nulling, harmonic detection, close to carrier noise, electron monitoring in the inner coaxial conductor [22], etc.

The sensitivity of the previous methods is not related to being global or local, as shown in Table I. It can be noted that some are very sensitive, thus detecting discharges that only change their output parameters by a factor of 5 and 10 dB, while others require a change of 10 dB or more. With specific attention on microwave nulling, it must be stated that its high sensitivity is only achieved when properly tuned and only for CW frequency, with sensitivity decaying rapidly when de-tuned or for modulated signals.

The novel detection system monitors the same parameters as the microwave nulling: RF signal at the fundamental frequency. But, instead of canceling two waves to obtain a null, it performs a statistical analysis of the measured in-phase and quadrature data. By fitting the data noise to a given model, it determines if the current measurement fits the model (no discharge) or does not (discharge).

The main benefits of the proposed method compared to the previous ones are that it does not require continuous tuning and that its sampling rate is higher (only limited by the RF equipment and system background noise). For comparison, the acquisition rate in this method goes beyond 40 MHz (see Section III), whereas it is limited to 1 kHz or less in the electron or light monitoring detection systems and to 3 MHz in the microwave nulling method [2]. So, due to its larger analysis bandwidth, this method is better suited to cope with small discharges (see Section III-D).

Also, this detection method provides the same sensitivity for CW signals, improves the accuracy when dealing with modulated signals—such as the ones used in [9] and [10]—and requires less RF components to set up. Furthermore, the proposed method benefits from its high detection rate. When operating the traditional microwave nulling system, the operator performs the "detection" by observing the signal analyzer. Even for skilled operators, the response time is no shorter than 1 sec. For the in-phase and quadrature (IQ) detection system [23]–[27], the execution time is shorter than 5 ms.

This work introduces the microwave nulling in Section II, since it is the predecessor. and monitors the same physical magnitudes as the proposed detection system. Next, the proposed IQ detection method is detailed in Section III. The experimental validation is carried out in Section IV, where it is applied to CW, analog modulated (chirp), and digitally modulated quadrature amplitude modulation (QAM) signals. Finally, Section V summarizes the main conclusions of this work.

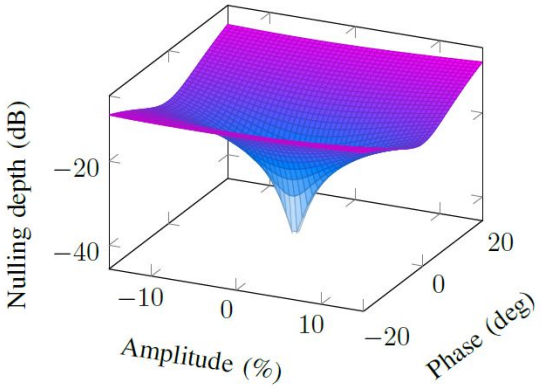

Fig. 1. Nulling depth in dB depending on the amplitude imbalance (%) and phase imbalance in degrees, clearly showing that small changes in amplitude, and specially in phase, will change the nulling detector output.

II. MICROWAVE NULLING

The microwave nulling [17] was designed to convert phase and amplitude variations into a scalar magnitude. Given that not many years ago vector signal analyzers were not so common, the signal phase information could not be directly measured. As RF breakdown produces more phase than amplitude changes, a physical mechanism to translate phase and amplitude imbalance into large amplitude changes was required.

This detection system is based on the out-of-phase addition of the equalized amplitudes of the forward and reverse signals. In an ideal signal case, the output of this addition should be zero and only the signal analyzer noise level would be measured. Due to the fact that non-ideal signals are being used, this sum has a very low level instead of zero. The maximum accuracy that can be obtained in a real microwave nulling system depends on the precision of the phase shifter and of the variable attenuator used to perform the counter-phase addition, as well as on the inherent noise of the signal source and power amplifier used for the signal generation and power amplification [2].

The main advantages of this method are: the high degree of sensitivity and the relative ease in its setting up. But its main drawbacks are: the need of being constantly re-tuned, its narrowband nature, the human intervention for discharge detection, and the cost of the involved RF passive equipment (especially if it is used exclusively for such tests). This detection method, which is still widely used in RF breakdown tests for CW and pulsed signals [2], is not fully suitable for modulated or multicarrier signals.

Fig. 1 shows the effect of the phase and amplitude imbalance in the nulling depth. From the plot, it is clear that small phase changes cause the detector output (nulling depth) to vary substantially. As the phase shifter is implemented with a transmission line of a variable length, this nulling depth

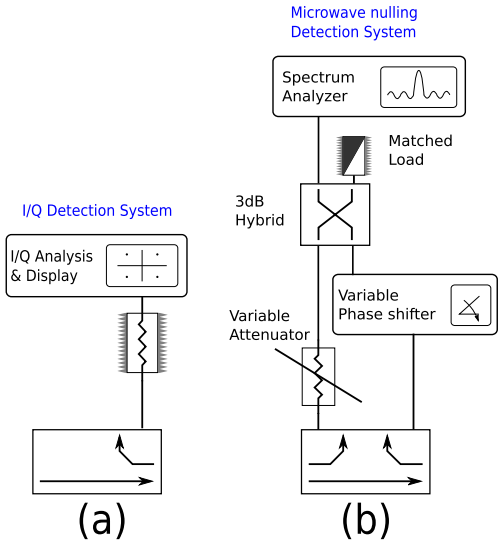

Fig. 2. Side-to-side comparison of the (a) IQ detection and the (b) microwave nulling implementations.

is only achieved at a single frequency. For modulated signals, only frequencies around the center one will have a sufficiently good nulling depth.

In a real implementation, temperature changes in the device under test (DUT), or amplifier gain impact on the amplitude modulation (AM) and phase modulation (PM) [28], make this imbalance larger over time, thus making it necessary to periodically adjust the nulling system.

Due to the strong push in digital communications for satellite and terrestrial applications, RF measurement technology has improved dramatically in recent years [9], [16]. Current hardware is capable of directly measuring the amplitude and phase information, known as IQ data, with high accuracy. But the microwave nulling system only measures scalar data.

In terms of physical implementation, Fig. 2 shows both methods side to side. It is clear, from the figure, that less hardware is required in the proposed detection system. For a test laboratory, less hardware implies lower cost and less chances of having RF connection issues.

The next section introduces the novel method in which IQ measurements and data processing are used to detect the presence of RF breakdown. The inputs of this new detection system are the same as for the microwave nulling (i.e., RF signals in the test bed at the fundamental frequency). But, in this case, it does not require any signal preconditioning performed by passive components. The IQ detection method has the benefit that it shows a similar performance to the classic nulling system for CW and pulsed CW signals, but it also copes well with modulated and multicarrier signals of any type. The only requirement is that the measured signal bandwidth is smaller than the IQ analyzer bandwidth, which is not only determined by the equipment sampling rate, but also by its analog front-end limitations.

III. IQ Detection Method

The IQ detection method is based on the mathematical analysis of the in-phase and quadrature information of the high power RF signal. Its operation principle relies on the fact that the RF breakdown generates additional noise that overlaps the already present system background noise. For each new measurement, the algorithm determines if the measured noise is what should be expected (system background noise) or not (background noise plus RF breakdown noise).

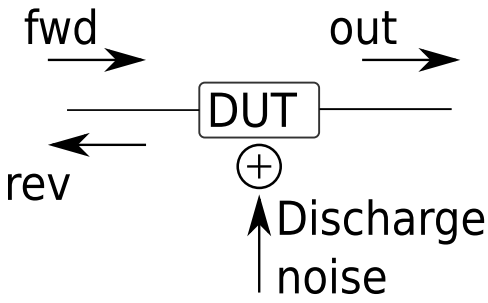

Fig. 3. Waves involved in a two-port device which can be acquired in order to detect the presence of the RF breakdown discharge.

The first step is to identify the noise sources in the test bed. Given that the propagation of the RF signal in a typical multipactor test bed is conducted (through coaxial or waveguide), the passive elements will not introduce extra noise, and the main noise sources will be the signal generator and the high power amplifier (HPA) [28]. For simplicity, the losses in the test bed are considered negligible. The signal-to-noise ratio (in dB) at the DUT input is defined as

$$\left(\frac{S}{N}\right)_{\text{fwd}} = \left(\frac{S}{N}\right)_{\text{gen}} - \text{NF}_{\text{HPA}} \tag{1}$$

where NF_{HPA} is the noise factor of the HPA. As the algorithm tries to identify the breakdown noise (N_{dsc}) out of the system ground noise (N_S), the path in which the system noise is lower is the one leading to a larger "breakdown noise" to "system background noise" ratio, thus improving the detection accuracy.

Under the scenario of a two-port DUT (see Fig. 3), there are three signals which can be measured at the DUT ports: forward, output, and reflected.

Following the signal path, the forward signal should not be significantly affected by the extra noise due to the discharge. For the reflected and output signals, the one showing a larger N_{dsc}/N_S ratio will depend on the DUT scattering parameters. Assuming a scenario in which the DUT is symmetrical, and the discharge happens at its middle point, the following equations define the noise at the reverse (N_{rev}) and output (N_{out}) paths:

$$\begin{aligned} N_{\text{rev}} &= N_S|S_{11}|^2 + 0.25N_{\text{dsc}}|S_{21}|^2 \\ N_{\text{out}} &= N_S|S_{21}|^2 + 0.25N_{\text{dsc}}|S_{21}|^2. \end{aligned} \tag{2}$$

From (2) it is clear that, as long as $|S_{11}| < |S_{21}|$, the discharge to system noise level will be larger in the reverse signal than in the output signal.

A. Noise Modeling

Once the location of the detection system with respect to the DUT has been defined, it is time to model the system noise. As the discharge noise has an unknown statistical distribution,

it is easier to model the normal system noise and use the hypothesis testing to verify whether the noise being measured fits the expected characteristics or not.

In this case, it is assumed that the in-phase and quadrature signals can be modeled as a Normal distribution. If the real and imaginary parts of the noise each follow a Normal distribution, then the error vector noise (EVN) calculated as the absolute value of the complex error follows a Rayleigh distribution.

A random variable $R \sim \text{Rayleigh}(\sigma^2)$ follows a Rayleigh distribution if $R = (I^2 + Q^2)^{1/2}$, where $I \sim N(0, \sigma^2)$ and $Q \sim N(0, \sigma^2)$ are Normal independent distributions. The Rayleigh PDF is

$$f_R(r;\sigma) = \frac{r}{\sigma^2} e^{-r^2/(2\sigma^2)}, \quad \sigma \approx \sqrt{\frac{1}{2N}\sum_{i=0}^{N} r_i^2}. \tag{3}$$

The hypotheses used to determine if there has been a discharge in a given measurement are (see Fig. 4) as follows.

1) H_0: There is no RF breakdown discharge.
2) H_1: There is an RF breakdown discharge.

RF breakdown detection occurs when H_1 is true and, moreover, H_1 is decided ($P_{\text{D}} = P\{H_1|H_1\}$). Nonetheless, false alarm RF breakdown occurs when H_0 is true but H_1 is decided ($P_{\text{FA}} = P\{H_1|H_0\}$). Since the probability density function (PDF) for the RF breakdown noise is not currently known, it is easier to calculate the false alarm probability instead of the detection probability (P_{FA}). Hence, in that case

$$P_{\text{FA}} = \int_{\eta}^{+\infty} f_{H_0}(\tau) d\tau \tag{4}$$

where f_{H_0} is the Rayleigh PDF defined in (3) and τ is the noise power.

In order to define the IQ detection method in a way that is closer to the microwave nulling system operation, instead of fixing a detection error (probability), a threshold η setting (in order to achieve a certain false alarm probability) provides a good compromise.

However, knowledge of the optimal η value requires some experience on test bed background noise and signal modulation. On top of that, a relevant standard to be followed is not available yet. Therefore, the procedure used here consists of estimating the EVN distribution using the concatenated EVN traces from the first N measurements, which are presumed not to have suffered from RF breakdown because the power level is low. From that large set of data, the EVN distribution is modeled, and η is determined from the false alarm probability (5). As the data has discrete values instead of continuous, the false alarm probability is given by

$$P_{\text{FA}} = \sum_{i=q}^{N \cdot P} \Delta\tau \cdot f_{H_0}(\tau_i) \tag{5}$$

where $\Delta\tau$ is the discretization interval, P is the number of points in each measurement, and q is the index position where $\tau = \eta$.

B. Signal Under Test

The RF signals used in this work have three parts which include, but are not limited to, the signal of interest. Due to the nature of RF breakdown testing, data throughput is not a critical requirement, so additional signal parts can be appended for the sake of a better detection performance. In particular, all the signals that have been experimentally validated are created by concatenating three segments whose purpose is very specific.

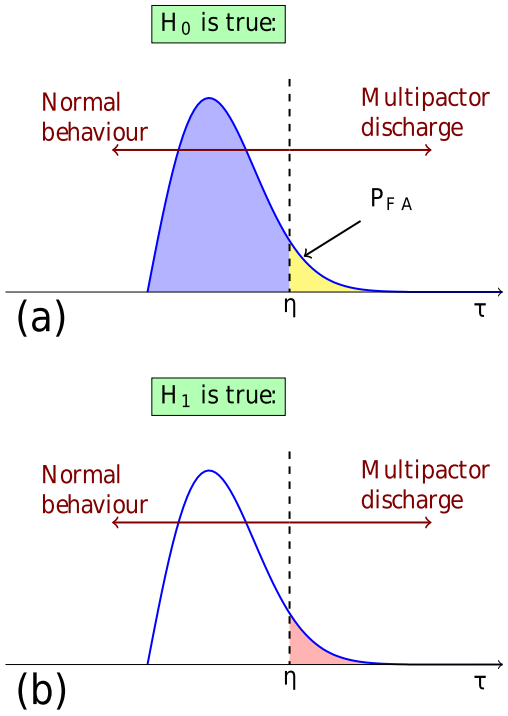

Fig. 4. Hypotheses tests. (a) Given that the noise PDF is not known, the hypothesis testing is done using H_0, which is assumed to follow a Rayleigh distribution. The probability of false alarm is the degree of freedom which determines the EVN threshold used for the RF breakdown detection. (b) Hypothesis testing using H_1 is not used as the multipactor noise distribution is not known.

The first segment (training segment) is used for amplitude normalization and phase alignment between the RF source and the analyzer, and for a frequency correction if required. The amplitude of this segment must be set to prevent RF breakdown discharge from occurring.

The second segment is an RF OFF interval, used to relax the electrons inside the RF device, so they lose kinetic energy and any already existing resonance.

The third segment is the actual signal of interest, which means the signal portion in which the RF breakdown must happen when increasing the RF power.

In this work, the time and amplitude characteristics of these three segments are: 1) Segment 1: RF ON with an initial CW signal (50-μs long) at -10 dBc and with 0° phase; 2) Segment 2: RF OFF (50-μs long); and 3) Segment 3: RF ON with the signal of interest (any length) with a peak level of 0 dBc. An example of this signal configuration is shown in Fig. 5.

Once a new acquisition is available ($s_{\text{in}}(t)$), the complete signal is normalized ($s_{\text{out}}(t)$) before computing the EVN. The scaling factors, computed from the training segment ($s_T(t) = s_{\text{in}}(t)$ for $0 \leq t \leq 50$ μs), are obtained as follows: 1) amplitude scaling factor a_s computed so that $s_T(t)$ has

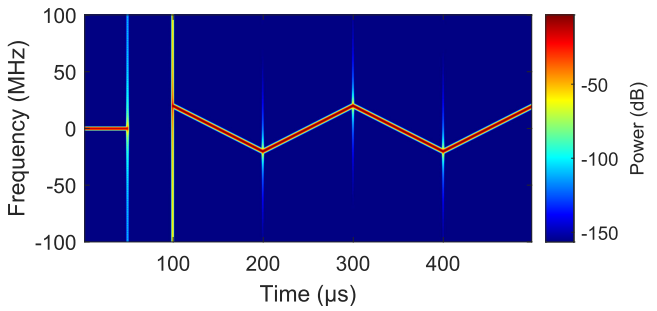

Fig. 5. Example of the three parts composing the typical signal structure used in this work. The signals start with an initial 50-μs CW pulse at -10 dBc used for calibration purposes. Next, there is a 50-μs interval with RF OFF for electron relaxation. Finally, the signal of interest is found at 0-dBc peak. In this particular example, the signal is an analog linear-frequency modulated chirp with two up-down intervals of ± 20 MHz each lasting for 100 μs.

1 V_{rms}; 2) phase correction factor θ_s: average phase of $s_T(t)$; and 3) frequency offset factors (θ_{fa} and θ_{fb}): obtained from the linear regression to $s_T(t)$ phase. Then, the normalized signal is computed as

$$s_{\text{out}}(t) = a_s s_{\text{in}}(t) \cdot e^{j\theta_s} e^{j(\theta_{fa}+\theta_{fb}t)}. \tag{6}$$

C. Reference Signal

Once the current measurement has been normalized, its EVN is obtained. The next question to solve is which reference signal, when used to compute the EVN, gives the best sensitivity for RF breakdown detection. This section discusses the reasons why the DUT input signal is not optimal for computing the EVN, and how the previous measured signals are stored in order to compute the reference signal.

Following the way in which the nulling system is implemented, it would make sense to use the input signal as the reference in order to compute the EVN. However, in practice, there are several considerations that do not support this approach: 1) it requires a second analyzer, which is expensive; 2) due to unequal frequency response in both paths (measurement and reference), the EVN would be larger if equalization is not used; and 3) there is a trigger jitter error between both devices.

For these reasons, the reference signal is defined as the average of the previous N measurements with no RF breakdown. In order to build this reference, a buffer spanning the N previous acquisitions is implemented in this work. The buffer follows a first in first out (FIFO) scheme, so once it is full, the oldest measurement is replaced by the newest one. This FIFO buffer follows the actual signal and, as the oldest traces are replaced, any possible distortion in the amplifier or the signal generator is taken into account.

From the authors' experience, the value for N is dependent on the HPA being used, system return losses, the DUT characteristics, and environmental parameters such as temperature. Therefore, there is not an optimal value for N which can be applied in all the possible scenarios.

Finally, once the current and reference signals are available, the EVN is computed as the difference between them.

D. Handling Small Discharges

Small discharges are difficult to handle in multipactor testing. Slow sampling rates in the local detection methods (about 1 kHz), and relative low sampling rate in the microwave nulling and harmonic detection systems (about 3 MHz), make them difficult to detect, as they are averaged out.

The small RF breakdown discharges can be classified into three groups: 1) fast events (in the order of ns) of moderate or even high amplitude; 2) moderate length events (<1 μs) of weak amplitude; and 3) fast events of weak amplitude.

Although from the perspective of the proposed algorithm, it always returns a statistically correct pass/fail result, and from the actual RF breakdown point of view, reliable results are to be expected mainly in cases 1 and 2. This is due to the larger acquisition bandwidth of this method, only constrained by the RF equipment, which provides more samples per second ($>$ 40 MHz). Nevertheless, small discharges of type 3 may, as it happens with all the other detection systems, be incorrectly detected or even missed.

In the experimental validation, it was observed that fast random values in the EVN were reported as discharges. At that stage, pulsed CW signals were being tested, which inherently could not suffer from extremely short discharges. This was confirmed by independent detection systems running in parallel, which did not record any discharge. For that reason, the algorithm was enhanced to require a minimum discharge length (i.e., certain amount of consecutive samples M failing the hypothesis test). This requirement ensures that random noise peaks, which do not fit the Rayleigh distribution but are not RF breakdown, do not produce a false detection. However, setting a large M value (i.e., >20) reduces the method responsiveness for small multipactor discharges.

Finally, the algorithm has the following three tuning parameters, which allow it to be either more responsive to small discharges or more robust against false detection: probability for the hypothesis test (η), number of consecutive samples failing the hypothesis test (M), and FIFO buffer size (N).

E. Algorithm Flowchart

The flowchart of the proposed detection algorithm is shown in Fig. 6. The threshold value (but not the false alarm probability) is updated during the test in order to take into account possible changes in the signal. In case RF breakdown is detected, the algorithm: 1) notifies the operator; 2) does not include the corresponding measurement in the buffer; and 3) reduces the RF power level (optional).

IV. Experimental Validation

This section presents the experimental validation of the proposed RF breakdown IQ detection system. Out of all the possible signals to be used in multipactor tests, the following ones have been selected: 1) pulsed CW; 2) linear frequency modulated CW (FM chirp); and 3) QAM digitally modulated signal.

The first signal, pulsed CW, is the standard waveform used in multipactor tests as defined in [17]. The FM chirp has been selected as the most interesting analog modulation for

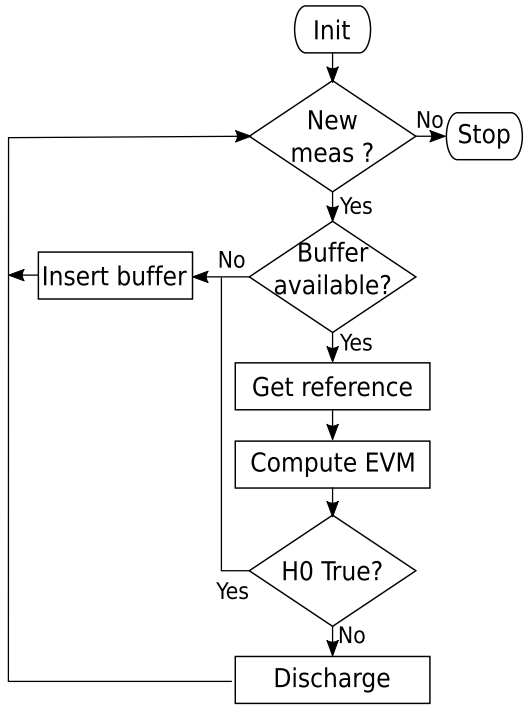

Fig. 6. Simplified IQ detection method flowchart. The management of the FIFO buffer is not detailed.

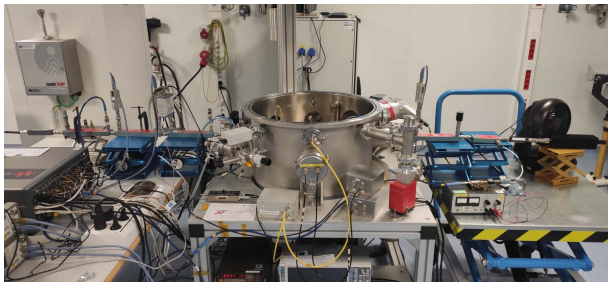

Fig. 7. Picture of the test bed, with the PXI chassis on the left, the TVAC on the center, and the output branch on the right. The test sample was installed in the TVAC.

space applications, being widely used in radar systems. Finally, the third signal is a very common digitally modulated signal.

The test bed was operated at L-band using very high-quality RF equipment, so that the detection is not compromised. Thus, a Keysight vector signal generator M9383A and a signal analyzer M9393A have been used, both with a sample rate of 200 MHz in order to cope with 160 MHz of IQ bandwidth. Both RF devices provide an amplitude flatness better than 0.5 dB and a deviation from linear phase $< \pm 1°$. The signal amplification was carried out with an R&S BBA150, which is a 1-kW solid state power amplifier (SSPA). The actual test bed is shown in Fig. 7, while Fig. 8 shows its schematic.

The multipactor reference sample is a reduced gap coaxial transmission line operating at L-band, with a multipactor threshold about 60-W peak for a CW signal. The sample threshold was verified with standard detection systems such as electron measurement, harmonic monitoring, and the classic nulling system (for the CW case). Periodic CW measurements were run between tests in order to detect any conditioning in the DUT. Harmonic and electron current monitoring systems were working all the time in parallel with the IQ detection.

For the following examples, the proposed method runs in about 1–2 ms, measured from the moment a new trace is received by the algorithm until a pass/fail decision in made. But the overall execution time is limited by the acquisition and trace transfer actions. For short signals ($<$300 μs), the complete execution time (including acquisition) is about 5 ms, although this time increments with the number of samples.

To obtain the maximum multipactor detection responsivity, the minimum discharge length should be set to 1. This requires a very low system noise, as if only one sample does not pass the hypothesis test, and then multipactor detection is triggered on.

In the validation stage, it was observed that, with the used setup, it was not possible to remove these short random noise events. As a consequence, several false detections were observed. In order to obtain robust multipactor detection, capable of handling these short errors, a minimum discharge length of $M = 10$ was found to be enough for this setup. This value remained the same for all the tested cases.

In terms of sensitivity, for the tested cases, the novel detection system recorded all the discharges simultaneously, i.e., same power step, or even before the harmonic and electron monitoring systems, which were running in parallel, as shown in Fig. 8.

A. Pulsed Continuous Wave

This signal scenario is the standard one in which the microwave nulling system shows its best performance. As defined in [17], the signal under test is a 20-μs CW pulse. As shown in Fig. 9, the residual EVN is better than -35 dB, which is a value comparable to the one that can be normally achieved in the nulling system when the operator is constantly tuning it, using a very precise phase shifter and a variable attenuator.

Fig. 10 shows how the response appears when there is an RF breakdown discharge with a clear increment in the EVN. This increment translates into the noise PDF which is shown in Fig. 11, where extra noise due to the RF breakdown discharge can be observed on the right-hand side of the figure.

B. Analog Modulation: FM Chirp

The next validation example consists of using an analog modulated signal. In this case, a chirp signal has been selected due to its constant power but linearly varying frequency. The chirp signal is the one shown in Fig. 5. The microwave nulling system cannot be used for this modulation type, as the signal only stays at a given frequency for a few time intervals along its whole duration. This implies that for most of the time, the nulling system would not be tuned at the chirp instantaneous frequency.

As depicted in Fig. 12, the response is not flat. This is due to the response of the passive elements, but also due to the RF generator (which is not pre-distorted). For this verification, the residual effect is not important and, indeed, adds value

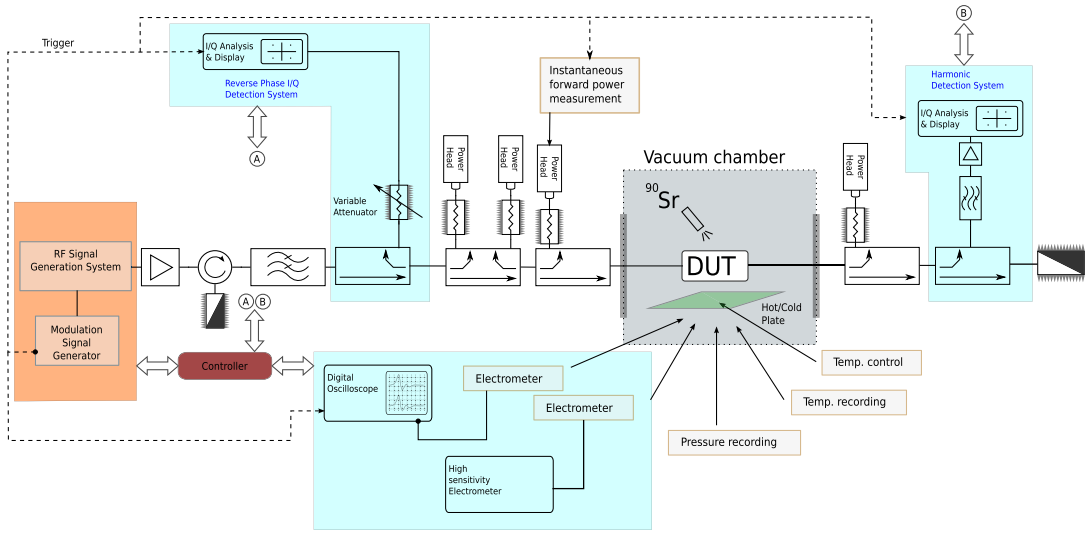

Fig. 8. Schematic of the test bed used for the IQ validation test campaign. During the initial threshold verification, the IQ detection system was replaced by the well-known microwave nulling system. The following detection methods were also continuously monitored during the validation of IQ detection system: RF harmonic detection system (1x, global) and electron monitoring (2x, local).

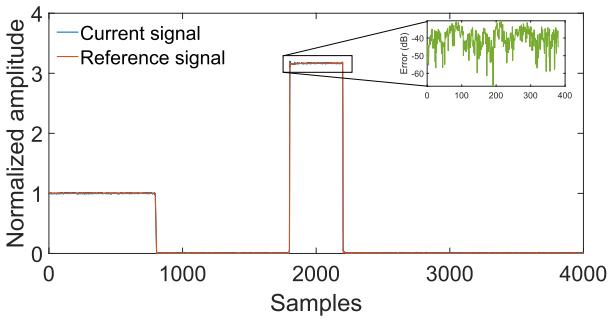

Fig. 9. Complete signal sequence for a CW payload in which there is no RF breakdown discharge. The small plot shows that EVN remains lower than −35 dB during the whole sequence.

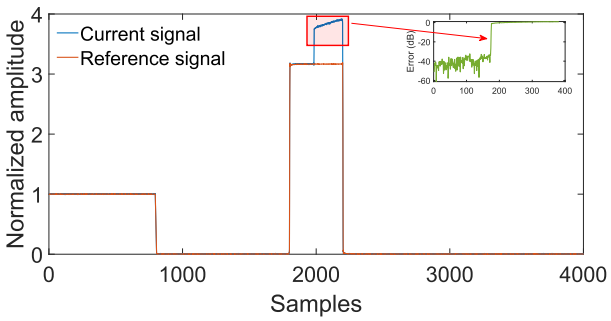

Fig. 10. Complete signal sequence for a CW payload in which there is an RF breakdown discharge. The small plot shows that EVN increases by 40 dB when the discharge happens.

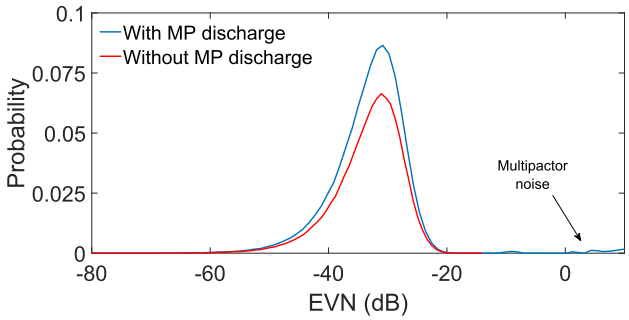

Fig. 11. PDF for the pulsed CW when there is a discharge and when there is not. The extra noise out of the Rayleigh distribution can be clearly identified on the right.

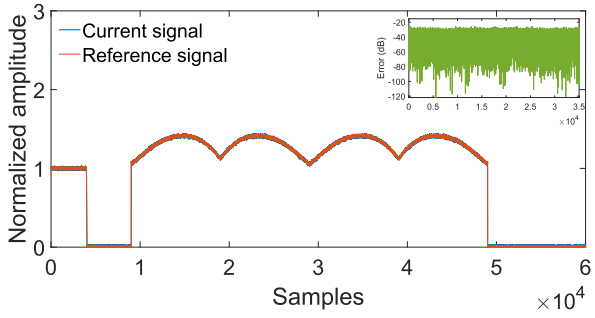

Fig. 12. Complete signal sequence for an FM chirp payload in which there is no RF breakdown discharge. The small plot shows that EVN remains lower than −30 dB during the whole sequence.

to the experimental results, as they show that the algorithm is able to cope with this residual AM. The EVN level is lower than −30 dB, which provides enough margin for reliable detection.

Fig. 13 shows how the response appears when the discharge happens and the corresponding increment in the EVN level. This response translates into the noise PDF which is shown in Fig. 14, where extra noise due to the RF breakdown discharge can be observed on the right-hand side of the figure.

C. Digital Modulation: QAM

The final validation is done with a QAM signal of 500-kHz bandwidth. These signals are not properly detected using the nulling system, due to its constant frequency and amplitude changes.

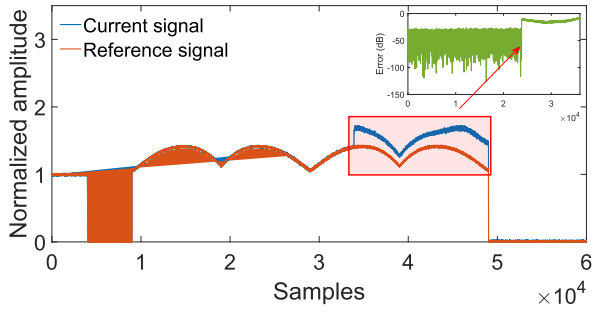

Fig. 13. Complete signal sequence for an FM chirp payload in which there is an RF breakdown discharge. The small plot shows that EVN increases by 20 dB when the discharge happens.

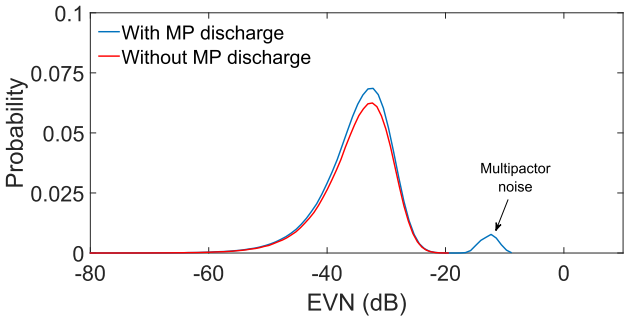

Fig. 14. PDF for the FM chirp payload when there is a discharge and when there is not. The extra noise out of the Rayleigh distribution can be clearly identified on the right.

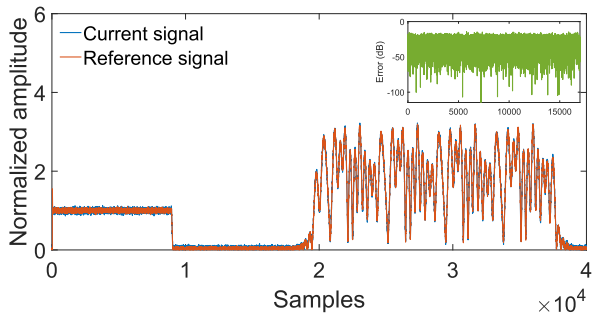

Fig. 15. Complete signal sequence for a QAM payload in which there is no RF breakdown discharge. The small plot shows that EVN remains lower than −30 dB during the whole sequence.

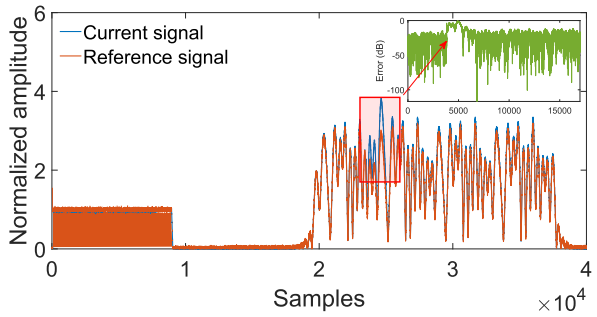

Fig. 16. Complete signal sequence for a QAM payload in which there is an RF breakdown discharge. The small plot shows that EVN increases by 20 dB when the discharge happens.

The EVN background level stays close to −30 dB as shown in Fig. 15. The effect of the multipactor discharge is shown in Fig. 16. This increment translates into the noise PDF which is shown in Fig. 17, where extra noise due to the RF breakdown discharge can be observed on the right-hand side of the figure.

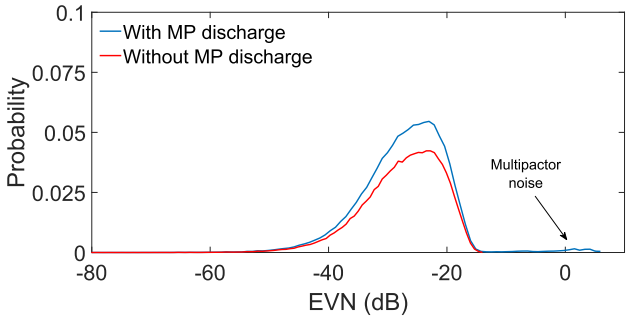

Fig. 17. PDF for the QAM payload when there is a discharge and when there is not. The extra noise out of the Rayleigh distribution can be clearly identified on the right.

V. Conclusion

This work has shown a novel high power RF breakdown detection technique, which surpasses the microwave nulling system while keeping its sensitivity and improving the related robustness and capabilities. The detection algorithm is based on the analysis of the signal noise using hypothesis testing. It has been experimentally validated with CW, analog, and digital modulated signals. The detection limitations of the technique are only constrained by the signal analyzer being used, which must be of high quality, and the test system residual noise level. These parameters will determine the residual EVN level, which must be as low as possible. The execution time of the proposed technique has proved to be about 5 ms or less.

Because of being a detection method which is not dependent on the manual adjustment of an operator and which provides quantitative results, it can be considered as a candidate for standardization in the RF breakdown testing field. It is important to note that it only relies on specifications and parameters that are set in advance and maintained during the complete RF test.

Finally, this testing approach, in which the signals are acquired and analyzed, allows the operator to store all the transmitted pulses, thus being possible to analyze them with other parameters or algorithms once the test has been completed.

References

[1] J. R. M. Vaughan, "Multipactor," *IEEE Trans. Electron Devices*, vol. ED-35, no. 7, pp. 1172–1180, Jul. 1988.

[2] A. Wood and J. Petit, "Diagnostic investigations into the multipactor effect, susceptibility zone measurements and parameters affecting a discharge," in *Proc. ESTEC Working Paper*, Nov. 1989.

[3] I. Arregui *et al.*, "High-power low-pass harmonic filters with higher-order TE_{n0} and non-TE_{n0} mode suppression: Design method and multipactor characterization," *IEEE Trans. Microw. Theory Techn.*, vol. 61, no. 12, pp. 4376–4386, Dec. 2013, doi: 10.1109/TMTT.2013.2288208.

[4] V. E. Semenov *et al.*, "Enhancement of the multipactor threshold inside nonrectangular iris," *IEEE Trans. Electron Devices*, vol. 65, no. 3, pp. 1164–1171, Mar. 2018, doi: 10.1109/TED.2018.2798538.

[5] J. Vague *et al.*, "Multipactor effect characterization of dielectric materials for space applications," *IEEE Trans. Microw. Theory Techn.*, vol. 66, no. 8, pp. 3644–3655, Aug. 2018, doi: 10.1109/TMTT.2018.2845869.

[6] J. Vague *et al.*, "Experimental validation of multipactor effect for ferrite materials used in L- and S-band nonreciprocal microwave components," *IEEE Trans. Microw. Theory Techn.*, vol. 67, no. 6, pp. 2151–2161, Jun. 2019, doi: 10.1109/TMTT.2019.2915546.

[7] S. V. Langellotti, N. M. Jordan, Y. Y. Lau, and R. M. Gilgenbach, "CST particle studio simulations of coaxial multipactor and comparison with experiments," *IEEE Trans. Plasma Sci.*, vol. 48, no. 6, pp. 1942–1949, Jun. 2020, doi: 10.1109/TPS.2020.2981257.

[8] M. A. Sanchez-Soriano *et al.*, "Study on multipactor breakdown in coaxial to microstrip transitions," in *IEEE MTT-S Int. Microw. Symp. Dig.*, Aug. 2018, pp. 1–4, doi: 10.1109/NEMO.2018.8503424.

[9] D. Gonzalez-Iglesias, O. Monerris Belda, M. E. Diaz, B. Gimeno, V. E. Boria, and D. Raboso, "Experimental analysis of the multipactor effect with RF pulsed signals," *IEEE Electron Device Lett.*, vol. 36, no. 10, pp. 1085–1087, Oct. 2015, doi: 10.1109/LED.2015.2468068.

[10] D. González-Iglesias *et al.*, "Analysis of multipactor effect using a phase-shift keying single-carrier digital modulated signal," *IEEE Trans. Electron Devices*, vol. 60, no. 8, pp. 2664–2670, Aug. 2013, doi: 10.1109/TED.2013.2266275.

[11] P. Martin-Iglesias, F. Teberio, and M. A. G. Laso, "Analysis of the multipactor effect with linear frequency modulated signals," in *IEEE MTT-S Int. Microw. Symp. Dig.*, Aug. 2018, pp. 1–4, doi: 10.1109/NEMO.2018.8503139.

[12] Á. Coves, G. Torregrosa-Penalva, C. Vicente, B. Gimeno, and V. E. Boria, "Multipactor discharges in parallel-plate dielectric-loaded waveguides including space-charge effects," *IEEE Trans. Electron Devices*, vol. 55, no. 9, pp. 2505–2511, Sep. 2008, doi: 10.1109/TED.2008.927945.

[13] *CST Particle Studio User Manual*, Dassault Systems, Vélizy-Villacoublay, France, 2020.

[14] V. Nistor *et al.*, "Multipactor suppression by micro-structured gold/silver coatings for space applications," *Appl. Surf. Sci.*, vol. 315, pp. 445–453, Oct. 2014.

[15] V. E. Semenov, E. I. Rakova, N. A. Zharova, J. Rasch, D. Anderson, and J. Puech, "Simple model of the RF noise generated by multipacting electrons," *J. Phys. D, Appl. Phys.*, vol. 47, no. 5, Feb. 2014, Art. no. 055206, doi: 10.1088/0022-3727/47/5/055206.

[16] O. M. Belda, E. D. Caballero, J. R. Garnica, and V. E. Boria, "Automatic, calibrated and accurate measurement of S-Parameters in climatic chamber," *IEEE Microw. Wireless Compon. Lett.*, vol. 25, no. 6, pp. 412–414, Jun. 2015, doi: 10.1109/LMWC.2015.2421330.

[17] *Multipaction Design and Test*, document ECSS-E-ST-20-01C, ESA-ESTEC, Jun. 2020.

[18] *Standard/Handbook for Multipactor Breakdown Prevention in Spacecraft Components*, document TOR-2014-02198 Aerospace Corporation, 28 May 2014.

[19] J. T. Farrell, T. E. Musselman, and A. A. Hubble, "Innovations in radio frequency breakdown detection methods," in *Proc. IEEE Int. Conf. Plasma Sci. (ICOPS)*, Jun. 2016, p. 1, doi: 10.1109/PLASMA.2016.7534164.

[20] R. Udiljak *et al.*, "New method for detection of multipaction," *IEEE Trans. Plasma Sci.*, vol. 31, no. 3, pp. 396–404, Jun. 2003, doi: 10.1109/TPS.2003.811646.

[21] H. Wei, X. Wang, W. Cui, Y. He, T. Hu, and Q. Sun, "Progress of multipactor detection in the space high-power microwave components," in *Proc. Int. Conf. Microw. Millim. Wave Technol. (ICMMT)*, May 2019, pp. 1–3, doi: 10.1109/ICMMT45702.2019.8992902.

[22] V. H. Chaplin, A. A. Hubble, K. A. Clements, and T. P. Graves, "Center conductor diagnostic for multipactor detection in inaccessible geometries," *Rev. Sci. Instrum.*, vol. 88, Jan. 2017, Art. no. 014706, doi: 10.1063/1.497434.

[23] L. Anttila, M. Valkama, and M. Renfors, "Frequency-selective I/Q mismatch calibration of wideband direct-conversion transmitters," *IEEE Trans. Circuits Syst. II, Exp. Briefs*, vol. 55, no. 4, pp. 359–363, Apr. 2008, doi: 10.1109/TCSII.2008.919500.

[24] R. Hassun, M. Flaherty, R. Matreci, and M. Taylor, "Effective evaluation of link quality using error vector magnitude techniques," in *Proc. Wireless Commun. Conf.*, Aug. 1997, pp. 89–94, doi: 10.1109/WCC.1997.622254.

[25] T. L. Jensen and T. Larsen, "Robust computation of error vector magnitude for wireless standards," *IEEE Trans. Commun.*, vol. 61, no. 2, pp. 648–657, Feb. 2013, doi: 10.1109/TCOMM.2012.022513.120093.

[26] K. Freiberger, H. Enzinger, and C. Vogel, "A noise power ratio measurement method for accurate estimation of the error vector magnitude," *IEEE Trans. Microw. Theory Techn.*, vol. 65, no. 5, pp. 1632–1645, May 2017, doi: 10.1109/TMTT.2017.2654221.

[27] R. A. Shafik, M. S. Rahman, and A. R. Islam, "On the extended relationships among EVM, BER and SNR as performance metrics," in *Proc. Int. Conf. Electr. Comput. Eng.*, Dec. 2006, pp. 408–411, doi: 10.1109/ICECE.2006.355657.

[28] O. Shimbo, "Effects of intermodulation, AM-PM conversion, and additive noise in multicarrier TWT systems," *Proc. IEEE*, vol. 59, no. 2, pp. 230–238, Feb. 1971.

Oscar Monerris-Belda received the M.Sc. degree in electric engineering from the Universitat Politècnica de Valencia, Valencia, Spain, in 2008, and coursed a specialization M.Sc. in 2009, and the M.Sc. degree in economics from the Universitat de València, Valencia, in 2014.

In 2010, he joined Val Space Consortium as a Technical Staff. His current research interests include high RF power effects in space applications, focusing in the analysis, testing, and detection of the RF breakdown in the presence of multicarrier and modulated signals.

Mr. Monerris-Belda has been a member of the Val Space Consortium Research and Development Board since 2020. He has also been a member of the Telecommunication Engineering Association in Valencia Board since 2016.

Raúl Cervera Marín was born in Valencia, Spain, in 1998. He received the bachelor's degree in telecommunications from the Universitat Politècnica de Valencia, Valencia, Spain, in 2020. He is actually pursuing the double M.Sc. degree in telecommunications.

Since 2021, he has been held a Junior Researcher position at Val Space Consortium. His current research interests include passive RF components, electromagnetic analysis, and RF breakdown power effects.

Miguel Rodríguez Jodar was born in Valencia, Spain, in September 1998. He received the bachelor's degree in telecommunication engineering from the Technical University of Valencia [Universitat Politécnica de València (UPV)], Valencia, in 2020, where he is currently pursuing the master's degree in telecommunications technologies, systems, and networks and the master's degree in telecommunications engineering.

His current research interests include multipactor prediction techniques for modulated signals and RF breakdown phenomena in collaboration with Val Space Consortium (VSC), Valencia, and the Technical University of Valencia.

Elena Diaz-Caballero received the bachelor's degree in telecommunication engineering and the M.Sc.Eng. and Ph.D. degrees from the Universitat Politècnica de València, Valencia, Spain, in 2010, 2011, and 2013, respectively.

In 2014, she joined Tesoro Imaging S.L., Valencia, a CSIC-UPV spinoff for the development of magnetic resonance imaging equipment. Since 2021, she has been a Math Professor. Her research interests include methods for the full-wave analysis and design of microwave devices, and biomedical RF applications.

Carlos Alcaide Guillén received the M.Sc. degree in telecommunication engineering and the Ph.D. degree in telecommunication engineering from the Universitat Politécnica de València (UPV), Valencia, Spain, in 2012 and 2019, respectively.

His current research interests include the improvement of the execution speed and the accuracy of multipactor simulations for microwave structures under the excitation of modulated signals.

John Petit received the B.Sc. degree in physics from the University of Sussex, Brighton, U.K., in 1980.

Since then, he has been working for a range of companies and institutions, covering the areas of defense, research, mobile systems, and space technology, which has included working at Marconi Company, Chelmsford, U.K., the University of Kent, Canterbury, U.K., COM DEV, Edinburgh, U.K., Honeywell U.K. Ltd., Bracknell, U.K., and ESTEC, Noordwijk, The Netherlands. His current position as a Senior Researcher is with Val Space Consortium, Valencia, Spain, where he is responsible for overseeing a three-year project funded by ESA, investigating multipactor prediction techniques in relation to GNSS signals. His principal experience is in the field of high power discharge effects, such as multipactor and gas breakdown in space components.

Mr. Petit is also a member of the Institution of Engineering and Technology, U.K.

Vicente E. Boria (Fellow, IEEE) was born in Valencia, Spain, in May 1970. He received the "Ingeniero de Telecomunicación" degree (Hons.) and the "Doctor Ingeniero de Telecomunicación" degree from the Universidad Politécnica de Valencia, Valencia, Spain, in 1993 and 1997, respectively.

In 1993, he joined the "Departamento de Comunicaciones," Universidad Politécnica de Valencia, where he has been a Full Professor since 2003. In 1995 and 1996, he was holding a Spanish Trainee position with the European Space Research and Technology Centre, European Space Agency (ESTEC-ESA), Noordwijk, The Netherlands, where he was involved in the area of EM analysis and design of passive waveguide devices. He has authored or coauthored 15 chapters in technical textbooks, 200 articles in refereed international technical journals, and over 250 papers in international conference proceedings. His current research interests include the analysis and automated design of passive components (in particular, filters and multiplexers) in several technologies, and the simulation and measurement of power effects in high-frequency devices and systems.

Dr. Boria has been a member of the IEEE Microwave Theory and Techniques Society (IEEE MTT-S) and the IEEE Antennas and Propagation Society (IEEE AP-S) since 1992. He is currently a member of the European Microwave Association (EuMA). He is also a member of the Technical Committee of the IEEE-MTT International Microwave Symposium and the European Microwave Conference. He has been the Chair of the 48th European Microwave Conference held in Madrid, Spain. He acts as a regular reviewer of the most relevant IEEE and IET technical journals on his areas of interest. He has been an Associate Editor of IEEE MICROWAVE AND WIRELESS COMPONENTS LETTERS from 2013 to 2018 and *IET Electronics Letters* from 2015 to 2018. He also serves as a Subject Editor (Microwaves) for *IET Electronics Letters* and an Editorial Board Member for *International Journal of RF and Microwave Computer-Aided Engineering*.

Benito Gimeno (Member, IEEE) was born in Valencia, Spain, in January 1964. He received the Licenciado degree in physics and the Ph.D. degree from the Universidad de Valencia, Valencia, Spain, in 1987 and 1992, respectively.

He was a Fellow with the Universidad de Valencia from 1987 to 1990. Since 1990, he has been serving as an Assistant Professor for the Departamento de Física Aplicada y Electromagnetismo, and the Instituto de Ciencia de Materiales (ICMUV), Universidad de Valencia, where he became an Associate Professor in 1997 and a Full Professor in 2010. He worked as a Research Fellow with the European Space Research and Technology Centre, European Space Agency (ESTEC-ESA), Noordwijk, The Netherlands, from 1994 to 1995. In 2003, he obtained a Fellowship from the Spanish Government for a short stay at the Universita degli Studi di Pavia, Pavia, Italy, as a Visiting Scientific. His current research interests include the computer-aided techniques for analysis of microwave and millimeter-wave passive components for space applications, waveguides, and cavities structures, including dielectric objects, electromagnetic band-gap structures, frequency selective surfaces, and nonlinear phenomena appearing in high-power high-vacuum microwave subsystems and particle accelerators as multipactor effect and RF breakdown. He is interested in the experimental study of secondary electron emission properties of metals, dielectrics, and ferrites. Recently, he is also involved in a research project oriented to the test of RF cavities used in Hadrontherapy systems for cancer treatment, and in the search of dark matter relic axions using microwave structures.

David Raboso was born in Spain, in 1967. He received the master's degree in physics from the University Autonoma of Madrid, Madrid, Spain, in 1992, and the master's degree in space engineering from the University of Delft, Delft, The Netherlands, in 2001.

In 1992, he started working at the European Space Agency, Noordwijk, The Netherlands, in the field of RF breakdown and passive intermodulation (PIM) within the payload systems division, at ESTEC, Noordwijk. In 2018, he became the Telecommunication Engineer honoris causa by the Polytechnic University of Valencia, Valencia, Spain. He is the coauthor in over 150 publications and the co-inventor in seven space-related patents.

Mr. David is currently the Chairperson of several European networks and working groups in the field of multipactor effect, corona, RF high power, and PIM. He is also responsible for the research and development and testing services area in RF breakdown at ESA. He has been participated in the organization of every MULCOPIM workshop since 1993 and in 2003 became the general chairman of this international event. Since 2010, he has been a manager of the European High Power RF Laboratory, Valencia, and the European High Power Space Materials Laboratory, Valencia.